A New Passive Boundary-Layer Control Device

M. Sajben,* C. P. Chen,† and J. C. Kroutil†
McDonnell Douglas Corp., St. Louis, Mo.

Experimental results show that a thin cylinder mounted near solid flow boundaries is capable of suppressing turbulent boundary-layer separation caused by adverse pressure gradients in subsonic flows. The cylinder is located parallel to the wall, normal to the flow, and several boundary-layer thicknesses away from the surface. Flowfield measurements suggest that the cylinder-wake/wall-boundary-layer interaction is responsible for the effects found. The ranges of geometrical and boundary-layer variables leading to improved performance were established for axisymmetric diffusers equipped with such devices. Empirical design rules are given. A comparison with vortex generators is made.

Nomenclature

A = cross-sectional area
b = weighting factor for index K_{ra2}
C_f = skin friction coefficient
C_p = $(p_w - \bar{p}_1)/\bar{q}_1$, wall pressure coefficient
C_{ps} = $(\bar{p}_2 - \bar{p}_1)/\bar{q}_1$, static pressure recovery
C_{pt} = $(\bar{p}_{t1} - \bar{p}_{t2})/\bar{q}_1$, total pressure loss coefficient
D = FCR diameter
F = axial force due to impulse of fluid leaving diffuser
H = δ^*/θ, shape factor
h = distance of FCR centerline from wall
K_ϕ = circumferential distortion index
K_{ra2} = radial distortion index
K_{a2} = combined distortion index
L = diffuser length
M = Mach number
$\dot{m}$ = mass flowrate through diffuser
p = pressure (time mean)
q = $\frac{1}{2}\bar{\rho}\bar{u}^2$, dynamic pressure
R = radius of cross section
Re = Reynolds number based on inlet diameter
t = FCR thickness
u = velocity (time mean)
x = axial coordinate
α = A_2/A_1, area ratio
δ = boundary-layer thickness $[u(\delta) = u_c]$
δ^* = $\int_0^R [1 - (\rho u/\rho_c u_c)](r/R)\,dr$, displacement thickness
ϕ = equivalent half-cone angle, defined by $\tan^{-1}\phi = (R_2 - R_1)/L$
ν = kinematic viscosity
ψ = force-based distortion index
ρ = density (time mean)
θ = $\int_0^R (u/u_c)[1 - (\rho u/\rho_c u_c)](r/R)\,dr$, momentum thickness

Subscripts

$0,1,2$ = plenum, model inlet, model exit locations, respectively
F = FCR location
S = separation point location in the absence of FCR
r = trip location
w = wall
c = core flow
a = ambient (atmospheric)
s = static
t = total (stagnation)
max = maximum
min = minimum

Superscripts

$'$ = root mean square of fluctuating component
$\bar{(\ )}$ = average over both time and cross-sectional area
$*$ = without FCR ("clean")

Introduction

EXTENSIVE evidence is presented to demonstrate that a thin cylinder mounted near solid flow boundaries is capable of delaying or eliminating turbulent boundary-layer separation caused by adverse pressure gradients. The cylinder is located parallel to the wall, perpendicular to the flow direction, and several boundary layers away from the surface. The device (named a flow control rail or FCR) is applicable to both internal and external flows. The present study concentrated on axisymmetric diffusers with both conical and smoothly curved contours. In this configuration, the FCR is a thin ring, generally located slightly downstream of the diffuser throat. Using area-averaged flow velocity, the nominal inlet Mach numbers were 0.28 and 0.58, and the Reynolds numbers based on diffuser throat diameter were 0.6×10^6 and 1.2×10^6.

The purpose of the study was to clarify the fluid mechanical processes involved, to establish the factors controlling the performance of the FCR, and to establish the magnitude of the improvements available.

The FCR was found to ensure attached, axisymmetric flow under a wide range of conditions that caused separation and transitory stall in "clean" diffusers. The absence of separation results in a more uniform and steady flow at the diffuser exit, which is desirable from the viewpoint of air-breathing propulsion system inlet efficiency and stability. The total pressure loss caused by the cylinder drag was generally offset by the gain from eliminating separation. The utility of the device lies in permitting shorter diffusers, or, in other applications, sharp, highly curved contours that otherwise would lead to separation. The simplicity of the device makes it attractive also as a fix or retrofit on existing surfaces. Because of the small dimensions of the FCR, the forces required to make it retractable should be achievable with lightweight components.

Application of the device was first proposed by Mattioli in 1932 for airfoil stall control and was successfully tested on the

Presented as Paper 76-700 at the AIAA/SAE 12th Propulsion Conference, Palo Alto, Calif., July 26-29, 1976; submitted Sept. 1, 1977; revision received March 10, 1977.

Index categories: Boundary Layers and Convective Heat Transfer – Turbulent; Nozzle and Channel Flow.

*Senior Scientist, McDonnell Douglas Research Laboratories. Associate Fellow AIAA.

†Research Scientist, McDonnell Douglas Research Laboratories.

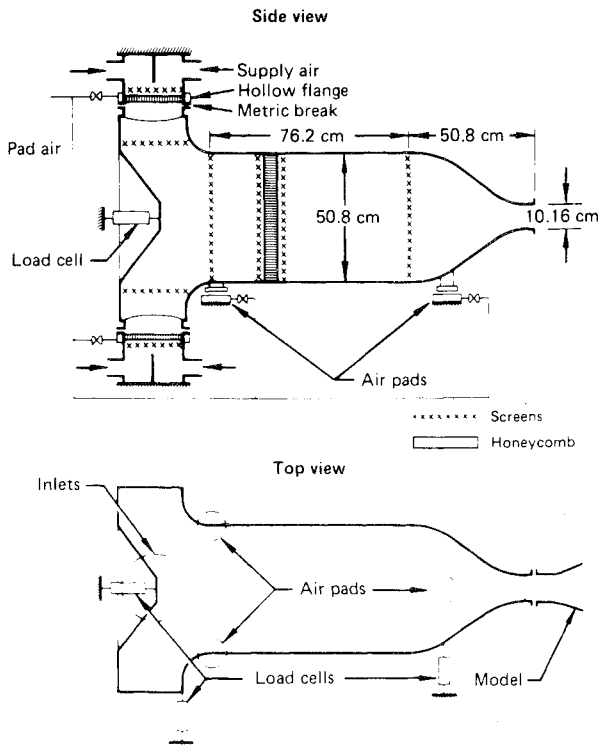

Fig. 1 Facility schematic (only the axial load cell was used).

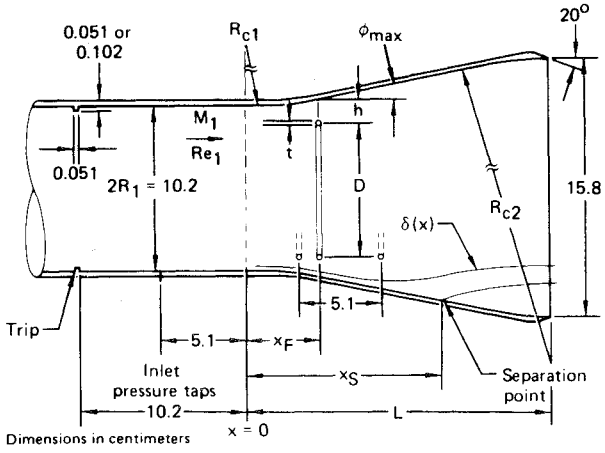

Fig. 2 Diffuser/FCR configurations tested; diffuser wall contour is composed of two straight and two circular arc line segments.

lower wing of a Caproni biplane.[1] The device apparently did not gain wide acceptance and only the accidental rediscovery by Moser in 1972[2] lifted it from oblivion. Application of the concept to internal flows, as reported here, is novel, and the empirical design information deduced from the present experiments is also new.

Experimental Apparatus

Experiments were conducted in the flow facility shown in Fig. 1. The facility is a plenum chamber of 51 cm diam, equipped with internal screens to produce uniform low-turbulence flow at the 10.2-cm-diam exit flange to which the models are attached. Provisions are available for accurate measurement of the axial force (thrust) caused by the impulse of the flow leaving the model. This force can be related to the flow distortion at the model exit, and its measurement was essential to the work reported here.

Exhaust is atmospheric, implying concurrent variation of Reynolds and Mach numbers. Flowrate is controlled by changing plenum pressure, the maximum being 2.3 kg/sec.

Table 1 Diffuser model dimensions[a]

Code	L/R_1	$2\phi/2\phi_{max}$[b]	R_{c_1}/R_1	R_{c_2}/R_1	x_r/R_1[c]
1	4.76	13/15	2.0	4.0	−2.0
2	4.0	16/18	2.0	4.0	−2.0
3	3.36	19/23	2.0	4.0	−2.0
4	2.83	22/31	2.0	4.0	−2.0
5	4.0	16/16	0.5	0.0[d]	−1.0

[a] All diffusers have an inlet diameter of 10.2 cm and an area ratio of 2.43.
[b] ϕ_{max} is illustrated in Fig. 2.
[c] Unless otherwise noted, the 0.051-cm high trip was used.
[d] Contour is a straight line to the exit.

Table 2 FCR dimensions

Code	Thickness (cm)	Diameter (cm)
1	0.203	7.62
2	0.203	8.26
3	0.203	8.89
4	0.203	9.53
5	0.160	7.62
6	0.160	8.26
7	0.160	8.89
8	0.160	9.05
9	0.160	9.53
10	0.160	10.16
11	0.160	10.80
12	0.160	12.07
13	0.079	7.62
14	0.079	9.53
15	0.079	10.16
16	0.079	11.43

The facility is complemented with appropriate instrumentation as well as data recording and processing equipment. Detailed description of the facility can be found in Refs. 3 and 4.

The models used were axisymmetric diffusers, chosen for the following reasons: 1) simple boundary shapes, 2) simple fabrication, 3) no serious space limitations on probe actuators, and 4) good match to the above described facility. Five diffuser models (all having an area ratio of 2.43) and sixteen FCR rings were used in various combinations, as shown in Fig. 2 for a general case. Dimensions are given in Tables 1 and 2.‡

Principal geometric variables were the following: 1) diffuser length (or angle), 2) FCR thickness, 3) FCR diameter, and 4) axial position of FCR. Considerable test time was saved by using an actuator suitable for moving the FCR in the axial direction over a range of 5.1 cm. The ring position could thus be varied during runs, and measured quantities could be plotted directly as a function of position with the aid of an *x-y* plotter. The rings were mounted on four thin lugs located 90° apart, with flat sides parallel to the flow to minimize frontal area.

Static pressure taps to measure wall pressure distributions were provided at 32 streamwise stations on model Nos. 1 to 4 and at 18 stations on model No. 5. Single roughness-element trips were used upstream of the model to produce turbulent boundary layers. The trips presented a square-wave-shaped obstacle to the flow and extended 0.51 and 1.02 mm above the wall surface, respectively.

‡Diffuser/FCR combinations will be designated by a symbol of the form *f/g*, where the code numbers *f* and *g* are given in the first columns of Tables 1 and 2, respectively.

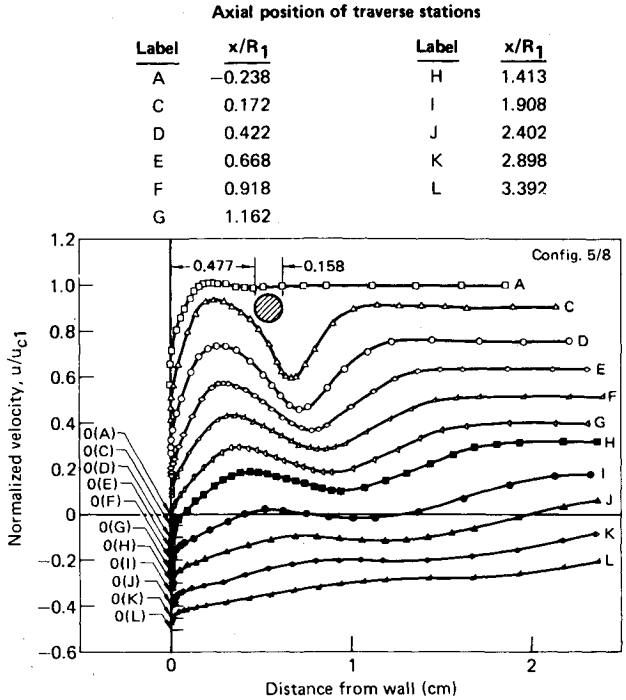

Fig. 3 Mean velocity profiles in FCR-equipped conical dissuser; $\bar{M}_1 = 0.25$. Note origin shifts.

Total pressures were measured at the diffuser exit with the aid of a total pressure tube rake. The rake had eight radial arms spaced 45° apart, each equipped with six total pressure tubes, located at radii of 3.0, 4.2, 5.2, 6.0, 6.7, and 7.3 cm. An additional tube was located on the axis, for a total of 49. Dimensions of the total pressure tubes were 0.81 mm o.d. and 0.41 mm i.d. The tubes were connected to a Scanivalve and a data recording system.

One of the diffusers (No. 5) was designed to accept miniature hotwire probes at 12 axial stations; the probes were mounted on a micrometer screw positioner with a 2.5 cm travel. A hotwire set (Thermo-System model 1050) was used to obtain mean velocity and turbulent intensity profiles.

Inlet Flow Conditions

Since diffuser flows are known to be sensitive to inlet velocity profiles, these were determined for both trip configurations. For the low flowrate ($\bar{M}_1 = 0.28$) the profiles were measured with a hotwire anemometer, while for the high flowrate ($\bar{M}_1 = 0.58$) a miniature total pressure probe was used. Data were evaluated by assuming constant static pressure and constant temperature across the boundary layer. The traverses were made in model No. 5 at $x = -1.2$ cm.

The measured velocity profiles (not given here) closely approximate distributions known to exist in zero pressure gradients at comparable Reynolds numbers. Calculated integral thicknesses are summarized in Table 3.

Table 3 Inlet boundary-layer properties

Trip height	$\bar{M}_1 = 0.28$	$\bar{M}_2 = 0.58$
0.51	$\delta^* = 0.41$	0.36
	$\theta = 0.28$	0.24
	H = 1.43	1.49
	$u_{c1}\ell/\nu = 1790$	3330
1.02	$\delta^* = 0.43$	0.43
	$\theta = 0.30$	0.30
	H = 1.44	1.43
	$u_{c1}\theta/\nu = 1880$	4170

All dimensions in mm.

The near equality of the boundary-layer thicknesses for the two trips was a surprise. The small difference may be due to the fact that the two layers are in different stages of their development: in terms of trip height, the distances to the traverse station differ by a factor of two.

Outside the boundary layer, the core flow velocity was uniform within 1% and the turbulence intensity was approximately 0.3%.

Phase I. Flowfield and Wall Pressure Measurements

The first phase of the investigation explored some flowfield details in a reasonably effective diffuser/FCR configuration, in order to obtain some insight into the nature of the fluid mechanic processes present. Hotwire measurements of mean and fluctuating velocity components were made in diffuser No. 5 without and with an FCR. The configuration for the second case was 5/8, with $x_F = 0.0$ cm.

The clean diffuser was separated in a nonaxisymmetric, unsteady mode (transitory stall). At the circumferential position of the hotwire stations, the separation point was near station H. Figure 3 shows data with the FCR installed. The wake of the cylinder and the parallel turbulent boundary layer are originally distinct, then interact with each other, and finally merge into a joint shear layer that remains attached throughout the diffuser. The shape factor (H) distributions computed from these data (Fig. 4) show that the rapid rise exhibited by the clean diffuser before separation is altered to a gradual growth by the FCR. (δ^* and θ were computed by integrating from the wall to the core flow regardless of profile shape.)

Another measure of the influence exerted by the FCR wake on the boundary layer is the increase of skin friction, which was obtained from Clauser plots using velocity maxima near the wall as u_∞. A reasonably well recognizable logarithmic segment exists in the velocity profile. The results indicate a roughly threefold reduction of the slope of a C_f vs x/R_1 plot, from -0.003 to -0.001. When the FCR is installed, C_f stays positive at all stations.

Measured turbulence intensity (u') distributions show that the FCR creates several times greater peak u' values than those originally present in the boundary layer at the FCR location. However, this turbulence decays and diffuses rapidly further downstream, whereas the boundary layer of the clean diffuser continues to grow more turbulent, with u' becoming extremely large past the point of separation. The peak turbulence intensity at the exit of the clean model is three times greater than that of the FCR-equipped diffuser, which suggests that the FCR probably attenuates dynamic distortion as well as static distortion.

Comparison of hotwire signals taken at the diffuser exit suggests that the FCR largely eliminates the large-amplitude, low-frequency (below 4 Hz) fluctuations evident in the clean model. Wall pressure distributions were measured for con-

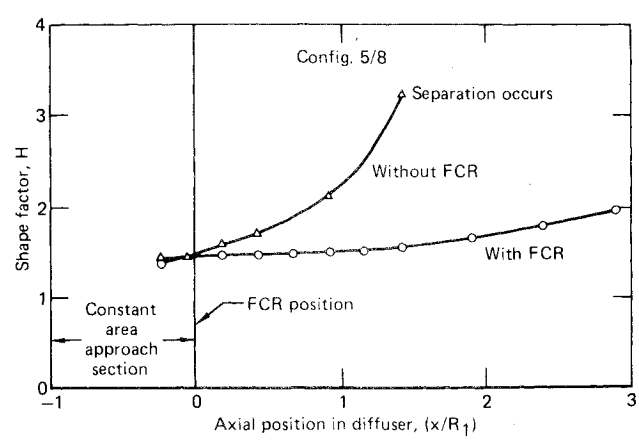

Fig. 4 Shape factor development with and without FCR; $\bar{M}_1 = 0.25$.

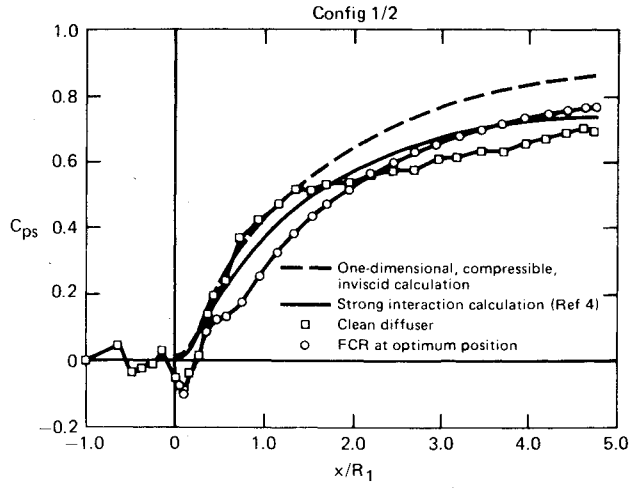

Fig. 5 Wall pressure distributions at $\bar{M}_1 = 0.58$.

figurations 2/2 and 3/2, each for two flowrates and four axial FCR positions. Figure 5 shows a typical case with and without the FCR and includes predictions by inviscid one-dimensional compressible theory and by the strong-interaction theory of Bower.[5] The plot shows that: 1) near the throat of the clean diffuser, the pressure rises steeply but the gradient is abruptly reduced at a point where separation is believed to occur; and 2) with the FCR in its "optimal" position, the pressure rise is gradual throughout the diffuser, without any sudden changes, and reaches a higher level than was attained in the clean model.

Phase II. Screening Tests

The second phase of the investigation explored promising ranges of geometric parameters at various pressure gradients, inlet boundary-layer thicknesses, and inlet Mach numbers. The screening was based on two readily measurable performance parameters. The first one is the static pressure recovery (C_{ps}), defined as the static pressure rise in the diffuser divided by the dynamic pressure based on mean inlet density and velocity. To characterize the nonuniformity of the velocity distribution at the diffuser exit, a distortion index (ψ_2) developed at MDRL was chosen as the second parameter. This index can be written as

$$\psi_2 \cong 1 + \frac{1}{A_2 \bar{\rho}_2 \bar{u}_2^2} \int_{A_2} \rho (u - \bar{u})^2 \, dA \qquad (1)$$

The precise definition, measurement, and interpretation of ψ_2 are given in Refs. 3 and 4, and a summary is presented in the Appendix. This index correlates well[6] with the widely used distortion parameter defined as $(p_{t\max} - p_{t\min})/\bar{p}_t$. For the purposes of this discussion, the two are considered equivalent (although not numerically equal).

The ψ_2 index was chosen for the present study, because it is proportional to the axial force which can be sensed by a single load cell. The real-time analog signal from the load cell, and two other appropriate pressure signals were manipulated in a manner corresponding to Eq. (A3) of the Appendix and as shown in Fig. 6 to produce instantaneous outputs proportional to C_{ps} and ψ_2. In conjunction with the capability to translate the FCR during each run, C_{ps} and ψ_2 vs x_F plots of the type shown in Fig. 7 could be obtained on a two-pen x-y plotter.

For a particular case, Fig. 7 shows that the improvement increases with axial distance from the diffuser inlet, up to approximately $x_F/R_1 = 0.43$, where the performance improvement is maximum and the flow is quite steady. If the FCR is moved further downstream, the flow separates, peformance decreases abruptly, and the flow becomes quite unsteady. The low-frequency components of the fluctuation

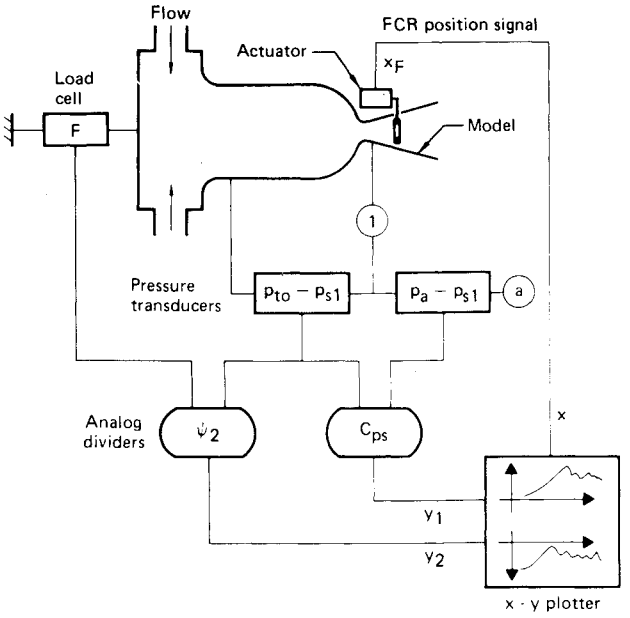

Fig. 6 Schematic of screening tests.

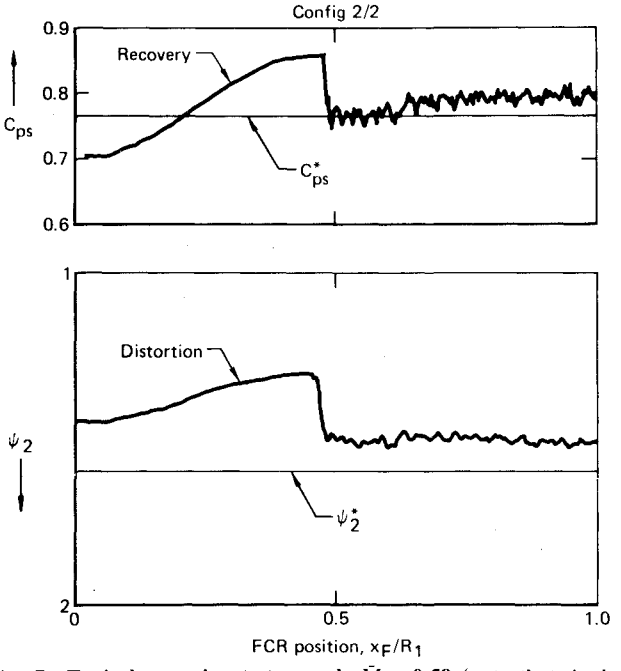

Fig. 7 Typical screening test record; $\bar{M}_1 = 0.58$ (note that ψ_2 increases downward to facilitate comparison with C_{ps}).

are substantial, as indicated by the ragged trace for both variables. Comparison of the traces with the horizontal lines representing the performance of the same diffuser without the FCR indicates that significant improvements were achieved for a range of axial FCR positions.

A total of 47 records similar to Fig. 7 were obtained and used to delineate the conditions for improved performance. The diffuser performance was considered improved when all of the following conditions were satisfied.

1) ψ_2^*: reduced distortion;
2) $C_{ps} > C_{ps}^*$: increased static pressure recovery;
3) the flow is steady, i.e., fluctuations similar to those in Fig. 7 (for $x_F/R_1 > 0.43$) are not present.

The results are summarized in terms of boundary-layer thickness and separation point location. Both were computed using the integral theory of Bower,[5] assuming the FCR to be absent. This theory considers a core flow at a uniform velocity

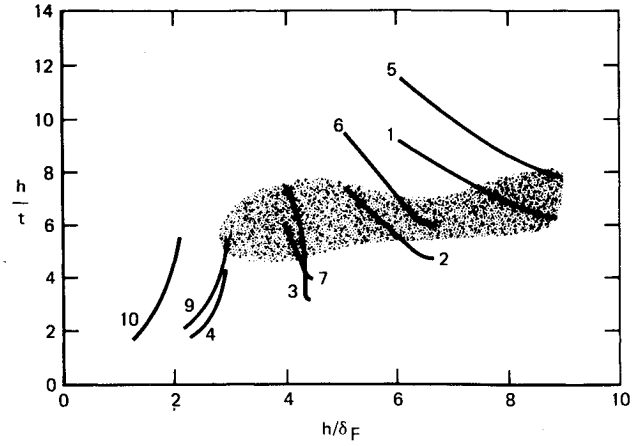

Fig. 8 Summary plot of screening test results for the no. 1 diffuser at $\bar{M}_1 = 0.28$. Curve labels correspond to FCR code numbers in Table 2.

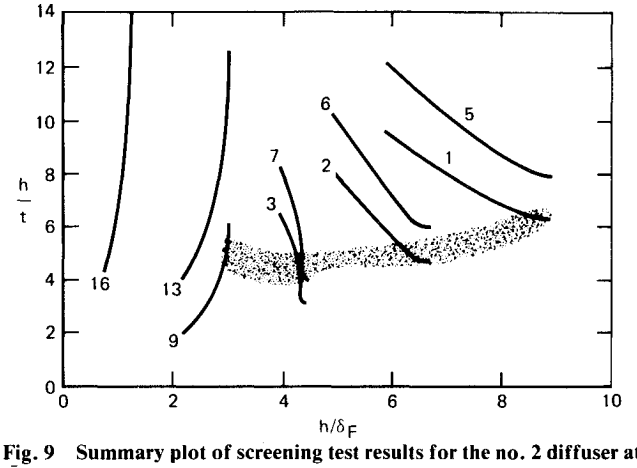

Fig. 9 Summary plot of screening test results for the no. 2 diffuser at $\bar{M}_1 = 0.28$. Curve labels correspond to FCR code numbers in Table 2.

u_c; the boundary-layer thickness δ is equal to the smallest y value for which $u(y) = u_c$. The reference thickness (δ_F) used in this report is the value δ at the FCR location in the absence of the FCR. The separation point location (x_S) is defined as the location where $H = \delta^*/\theta = 1.8$, also considering the FCR absent. If a more realistic velocity profile is considered, featuring a gradual approach to u_c (such as might be obtained from a measurement), then δ may be taken as the y value where $u(y) = 0.99\ u_c$. Note that for a turbulent boundary layer, fully developed in zero pressure gradient, $\delta^* \approx 0.2\delta$ at $Re_\theta = 400$, gradually changing to $\delta^* \approx 0.14\delta$ at $Re_\theta = 15{,}000$.

The range of thicknesses t and the FCR-to-wall distances h for which performance improved are indicated in a h/t vs h/δ_F map (Fig. 8). Both δ_F and h vary during the axial traverse of the FCR, as do the normalized variables. Curved lines show the trajectories of the representative points over the map for various FCR's. Conditions covered by the lines (not all are hown) were explored, and improvements were found within the shaded region. Figure 8 shows the results for the 15° diffuser (No. 1), and Fig. 9 shows results for the 18° diffuser. Some improvements in distortion were found with the 23° and 31° diffusers (Nos. 3 and 4), but recovery was worse, indicating that the pressure gradients in these cases are too steep and exceed the capabilities of the FCR.

The FCR must be located upstream of the point where the separation would occur in its absence (x_S). Furthermore, the distance to the separation point must be sufficiently long to allow the wake/boundary-layer interaction to exert its influence. On the other hand, the wake effect would decay too soon if the FCR were placed too far upstream. These expectations are verified by the h/t vs $(x_S - x_F)/h$ maps given in Figs. 10 and 11, which were constructed in a manner analogous to the previous two figures.

As mentioned earlier, the increase of trip height from 0.051 to 0.102 cm caused a surprisingly small increase of the boundary-layer thickness. Several runs, made with model No. 2 at $\bar{M}_1 = 0.28$, verified the expectation that the FCR effects also differed little from results obtained with the 0.051-cm trip. Regions of improved performance were slightly smaller and contained within the envelopes shown in Figs. 9 and 11.

The magnitude of improvements found within the shaded regions is given in Table 4.

Design Rules

Figures 8-11 are consistent with the following set of simple design rules:

1) The distance from FCR to wall (h) should be from $4\delta_F$ to $8\delta_F$.

2) The FCR should be located from $5h$ to $7h$ upstream of the separation point for the flow without an FCR.

3) The FCR thickness should be about equal to δ_F.

Since x_F and δ_F are not known at the outset, the design procedure must start with the determination of $\delta(x)$ and x_s. The theory of Bower[5] is preferred for consistency, but others could be used. The next step is to prepare a $y(x)$ plot containing the curves defined as $y = 4\delta(x)$, $y = 8\delta(x)$ and the straight lines $y = -5(x - x_S)$ and $y = -7(x - x_S)$. Points inside the region enclosed by these four lines satisfy rules 1 and 2 and define the recommended placement for the FCR. Having chosen x_F and h within this region, t immediately follows by rule 3.

If calculated results are not available, the boundary-layer thickness and the separation point need to be determined experimentally in the neighborhood of the anticipated FCR location.

These rules should provide a reasonable definition of a trial configuration for test purposes. Further refinements would best be done by tests using the particular geometry of interest.

Phase III. Performance Measurements

Tests in the previous phase were a convenient and fast means to establish those values of controlling parameters that generally improve the flow. They did not, however, determine the extent of improvement in terms commonly used by designers, nor did they yield values directly comparable with existing data. In particular, the total pressure loss coefficient and some conventionally accepted distortion index are of direct interest. In order to compute such parameters, total pressure distributions were determined for two flow rates at the diffuser exit with the eight-arm rake, for 32 various diffuser/FCR configurations.

The data were used to compute the following performance variables: 1) total pressure recovery, $(\bar{p}_{t2}/\bar{p}_{t1})$, the ratio of area averaged total pressures at exit and inlet, 2) distortion index defined as

$$(p_{t\max} - p_{t\min})/\bar{p}_t \qquad (2)$$

Table 4 Largest improvement obtained for static pressure recovery and exit distortion using FCR's

Model No.	$\bar{M}_1$ = 0.28		$\bar{M}_1$ = 0.58	
	C^*_{ps}	$C_{ps} - C^*_{ps}$	C^*_{ps}	$C_{ps} - C^*_{ps}$
1	0.68	0.04	0.82	0.04
2	0.63	0.06	0.76	0.10
	$\psi^*_2 - 1$	$\psi^*_2 - \psi_2$	$\psi^*_2 - 1$	$\psi^*_2 - \psi_2$
1	0.35	0.18	0.54	0.27
2	0.40	0.20	0.60	0.34

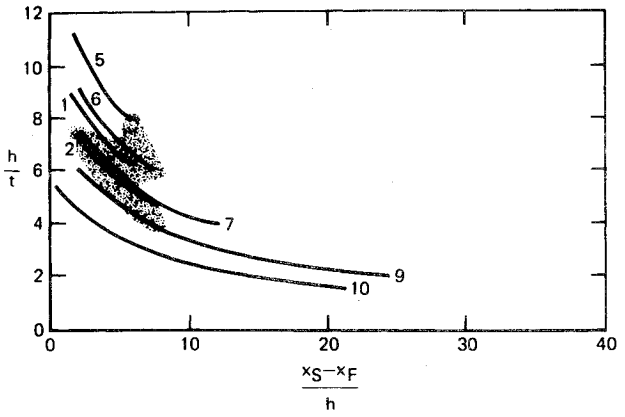

Fig. 10 Summary plot for axial FCR position; model no. 1, $\bar{M}_I = 0.28$. Curve labels correspond to FCR code numbers in Table 2.

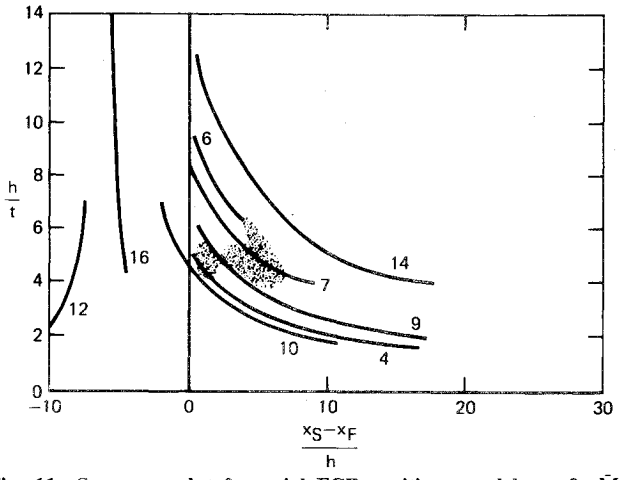

Fig. 11 Summary plot for axial FCR position; model no. 2, $\bar{M}_I = 0.28$. Curve labels correspond to FCR code numbers in Table 2.

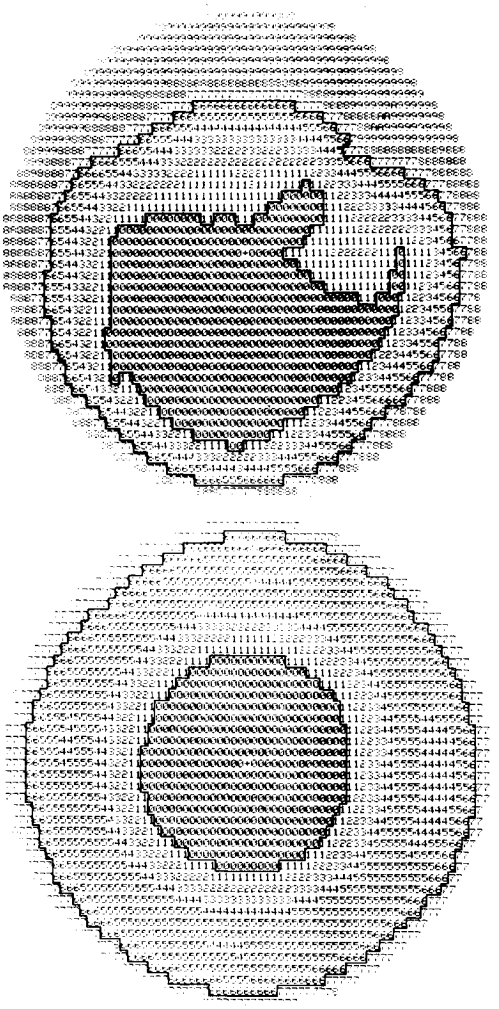

Fig. 12 Total pressure loss contour map at diffuser exit for model no. 1 without FCR (top) and with FCR no. 2 (bottom); $\bar{M}_I = 0.58$. Symbol 0 describes $C_{pt} < 0.05$; greater numbers stand for greater values, in successive increments of 0.05.

where the average $\bar{p}_t$ is the arithmetic average of the 49 readings, and 3) circumferential and radial distortion indices K_θ and K_{ra2}, developed by UTC Pratt & Whitney Division.[7]

K_θ is proportional to a linear combination of Fourier coefficients, computed from azimuthal pressure distributions measured at each fixed radius. The weighting coefficients are empirical.

K_{ra2} is computed from the radial distribution of circumferentially averaged total pressures, taking into account the radial distributions "preferred" by the compressor. Compressor stall can be predicted from a combined index defined as

$$K_{a2} = K_\theta + bK_{ra2} \tag{3}$$

where b is an empirical coefficient dependent on engine type and engine air flow.

The rake measurements were used to construct contour maps of the type shown in Fig. 12, which effectively show the FCR effects. In addition to the alphanumeric symbols describing the local loss coefficient values, lines corresponding to constant values of $C_{pt} = 0.05$ and 0.35 also are given to emphasize the nature of the distribution. The clean case shows a large low-energy zone at the top, corresponding to an intermittently separated region. Insertion of the FCR slightly reduces the core flow area, but the extent of the high-loss region (with codes 7 and greater) is also reduced, and by a much greater amount. The distribution also becomes nearly axisymmetic.

Integrated (area averaged) values of the total pressure recovery coefficient ($\bar{p}_{t2}/\bar{p}_{t1}$) were calculated and were found to be greater than values for clean diffusers by about 0.5%. As anticipated from Fig. 12, the greatest improvement occurs in terms of circumferential distortion as demonstrated by the K_θ values of Fig. 13. K_θ reductions up to an order of magnitude were obtained; K_{ra2} values were decreased by 15 to 30%. The significance of these results depends primarily on the response of the engine to various types of inlet distortions; application of the FCR would be most profitable in connection with an engine primarily sensitive to azimuthal variations.

FCR vs Vortex Generators

No definitve comparisons could be made between the present FCR results and data available on vortex generators from the literature because of differences in relevant test variables or in measured performance parameters. Most published studies were restricted to static pressure recovery measurements, and comparison can therefore be made only in terms of C_{ps}.

Properly designed FCR's can improve static recovery by ΔC_{ps} ($= C_{ps} - C^*_{ps}$) values of 0.03 to 0.10, as shown in Table 4. Vortex generators in a conical diffuser have been demonstrated to produce somewhat better results, although the available data refer to different diffuser shapes. Taylor[8] reports experiments on diffusers with $\alpha = 5.2$, whose recovery at $2\phi = 13°$ and 16° could be improved by $\Delta C_{ps} = 0.15$ and 0.20, respectively. Valentine and Carroll[9] report test results on a $2\phi = 23°$, $\alpha = 2$ diffuser, giving ΔC_{ps} values up to 0.2 for various vortex generator configurations. Both the Taylor and

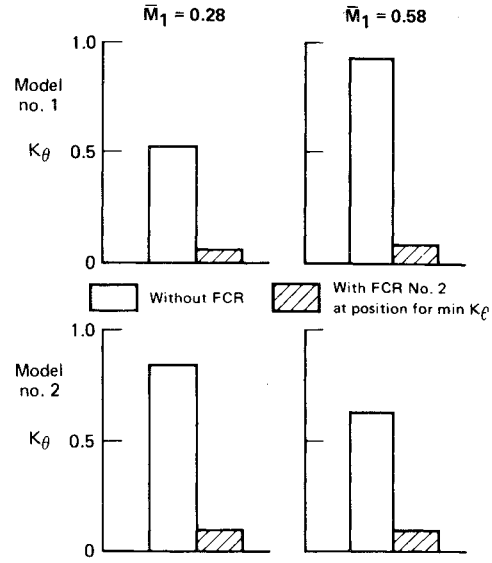

Fig. 13 Circumferential distortion index values measured with and without an FCR.

Valentine experiments were at an order of magnitude greater Reynolds number than those in the tests presented herein.

Senoo[10] reports ΔC_{ps} values up to 0.2 at $\alpha = 4$, but the co-rotating arrangement of the vortex generators he used introduces considerable swirl which alone might account for much of the improvement.[11] Swirl-free arrangements of vortex generators yielded ΔC_{ps} results of -0.1 to 0.15, depending on diffuser cone angle.

No static pressure recovery information was found on diffusers directly comparable with our models. Likewise, no reliable total pressure loss information was found for any comparable conical or contoured axisymmetric diffuser configuration with vortex generators.

As discussed previously, the FCR performed best in terms of reducing exit distortion. Unfortunately, no specific distortion data were found for vortex generator experiments; however, velocity profiles measured at the exit of the vortex-generator equipped diffuser[9] show velocity peaks presumably associated with the presistent streamwise vortices shed from the generator. No such "ripples" were found in FCR tests; the cylinder wakes completely merged with the wall boundary layer within the diffuser. Neither device should be expected to benefit originally unseparated flows.

The FCR is most effective in attenuating distortion and warrants serious consideration especially when the smoothing of circumferential nonuniformities is a primary objective. Also, because of its simplicity, the FCR is inexpensive to design, fabricate, modify, and retrofit, and may therefore have an advantage over vortex generators when cost and weight are dominant considerations; even a retractable FCR configuration would be light in view of the small actuator forces required.

Summary

Flow control rails were shown to be a simple means of suppressing separation of turbulent boundary layers in subsonic flows with moderately strong adverse pressure gradients. In the context of air induction systems, the FCR can be used to reduce steady-state and probably also dynamic distortion at the compressor face. Improvements in flow uniformly were demonstrated for simple diffuser configurations. Simple design rules, developed in terms of boundary-layer variables, are expected to apply for a wide range of configurations.

The investigation showed that large-scale wake turbulence, introduced into the freestream at a considerable distance ($\sim 6\delta$) from the wall can reduce the tendency of the boundary layer to separate. This fact might be purposefully exploited in cases where a turbulent wake necessarily exists near boundary layers, such as slat wakes over airfoils or airfoil wakes over flaps.

Appendix

Test facilities originally intended for the measurement of thrust (i.e., axial force resulting from the exit impulse of the flow) can also be used to measure the degree of flow distortion at the model exit. An index can be defined as follows:

$$\psi_2 = \bar{\rho}_2 A_2 F_2 / \dot{m}^2 \tag{A1}$$

The force F is equal to the impulse function $(p+\rho u^2)$ integrated over the exit cross section. If the exit is atmospheric, the contributions from static pressure are small and the force is proportional to $(\rho u^2)_2$. Furthermore, $\dot{m}$ is proportional to $\bar{\rho}_2 \bar{u}_2$. Equation (A1) can therefore be written as

$$\psi_2 - 1 = (1/A_2 \bar{\rho}_2 \bar{u}_2^2) \int_{A_2} \rho (u-\bar{u})^2 \mathrm{d}A \tag{A2}$$

The expression on the right-hand side is zero if the velocity profile is flat and increases with increasing nonuniformity. (Note that the integrand is always positive.)

A simple measurement of ψ_2 is possible if the exit Mach number is low (≤ 0.3). In this case, $\dot{m}^2/\bar{\rho}_2$ is proportional to $\frac{1}{2}(\bar{\rho}_1 \bar{u}_1^2)$, which is nearly equal to the difference of plenum and throat static pressures. Thus,

$$\psi_2 \cong \alpha^2 F / 2A_2 (p_{t0} - p_{s1}) \tag{A3}$$

The load cell signal and the signal from a differential pressure transducer can be used with a ratio meter to obtain a real-time, analog signal proportional to exit distortion.

Acknowledgment

This work was conducted under the McDonnell Douglas Independent Research and Development Program.

References

[1] Anon., "To Improve Control at the Stall," *The Aeroplane*, Aug. 1934, pp. 256-257.

[2] Moser, A., "Experimental Investigation of Wake/Boundary Layer Interaction and The Flow Control Rail," McDonnell Douglas Report MDC Q0511, Dec. 1973.

[3] Sajben, M., Kroutil, J. C., Sedrick, A. V., and Hoffman, G. H., "Experiments on Conical Diffusers with Distorted Inflow," AIAA Paper 74-529, Palo Alto, Calif., 1974.

[4] Sajben, M., Kroutil, J. C., and Sedrick, A. V., "Performance and Exit Distortion of Diffusers as Determined by Force Measurements," McDonnell Douglas Research Laboratories, Paper MDRL 74-2, 1974.

[5] Bower, W. W., "An Analytical Procedure for the Calculation of Attached and Separated Subsonic Diffuser Flows," *Journal of Aircraft*, Vol. 13, Jan. 1976, pp. 49-56.

[6] Sajben, M., Chen, C. P., and Kroutil, J. C., "Comparison of Conventional and Force-Based Distortion Index Measurements," *AIAA Journal*, Vol. 14, Oct. 1976, pp. 1500-1501.

[7] Farr, A. P., "Evaluation of F-15 Inlet Dynamic Distortion," AIAA Paper 73-784, St. Louis, Mo., 1973.

[8] Taylor, H. D., "Summary Report on Vortex Generators," United Aircraft Corporation Rept. R-05280-9, 1950.

[9] Valentine, E. F. and Carroll, R. B., "Effects of Some Primary Variables of Rectangular Vortex Generators on the Static-Pressure Rise Though a Short Diffuser," NACA RM L52B13, 1952.

[10] Senoo, Y. and Nishi, M., "Improvements of the Performance of Conical Diffusers by Vortex Generators," *Journal of Fluid Engineering*, Vol. 96, Part 4, March 1974, pp. 4-10.

[11] McDonald, A. T., Fox, R. W., and Van Dewoestine, R. V., "Effect of Swirling Inlet Flow on Pressure Recovery in Diffusers," *AIAA Journal*, Vol. 9, Oct. 1971, pp. 2014-2018.